ilmedia

TECHNISCHE UNIVERSITÄT
ILMENAU

Becker, Tatiana; Stolbov, Oleg V.; Biller, Armin M.; Borin, Dmitry Yu.;
Stolbova, Olga S.; Zimmermann, Klaus; Raikher, Yuriy L.

Shape-programmable cantilever made of a magnetoactive elastomer of mixed content

Original published in:	Smart materials and structures. - Bristol : IOP Publ.. - 31 (2022), 10, art. 105021, 14 pp.
Original published:	2022-09-16
ISSN:	1361-665X
DOI:	10.1088/1361-665X/ac8f79
[*Visited:*	2023-05-05]

This work is licensed under a Creative Commons Attribution 4.0 International license. To view a copy of this license, visit https://creativecommons.org/licenses/by/4.0/

TU Ilmenau | Universitätsbibliothek | ilmedia, 2023
http://www.tu-ilmenau.de/ilmedia

OPEN ACCESS
IOP Publishing
Smart Materials and Structures
Smart Mater. Struct. **31** (2022) 105021 (14pp)
https://doi.org/10.1088/1361-665X/ac8f79

Shape-programmable cantilever made of a magnetoactive elastomer of mixed content

T I Becker[1,*], O V Stolbov[2], A M Biller[2], D Yu Borin[3], O S Stolbova[2], K Zimmermann[1] and Yu L Raikher[2,*]

[1] Technical Mechanics Group, Faculty of Mechanical Engineering, Technische Universität Ilmenau, 98684 Ilmenau, Germany
[2] Institute of Continuous Media Mechanics, Russian Academy of Sciences, Ural Branch, 614018 Perm, Russia
[3] Chair of Magnetofluiddynamics, Measurement and Automation Technology, Institute of Mechatronic Engineering, Technische Universität Dresden, 01062 Dresden, Germany

E-mail: tatiana.becker@tu-ilmenau.de and yuriy.raikher@gmail.com

Received 8 June 2022, revised 13 August 2022
Accepted for publication 4 September 2022
Published 16 September 2022

Abstract

This work presents an approach to the macroscopic field-controlled mechanics of magnetoactive elastomers of mixed content, which are a special type of smart materials made of an elastic composite and a combination of two essentially different ferromagnetic fillers. High-coercive particles of NdFeB-alloy powder for the magnetically hard (MH) filler and carbonyl iron powder particles with nearly zero coercivity for the magnetically soft (MS) filler are usually used. The MH particles are tens-of-micron in size and impart to the elastomer a remanent magnetisation, whereas due to the MS particles of several microns in size, the elastomer acquires a high magnetic susceptibility. Since large MH particles once magnetised in a strong field possess their own fields to which the MS particles are susceptible, the overall elastomer magnetisation as well as its mechanical response greatly depends on the relative concentration of both fillers. This work particularly studies the bending deformation of horizontally fixed magnetoactive cantilevers with the permanent magnetisation along the length axis under the action of gravity and a vertically applied uniform magnetic field. The cantilevers of the same geometry and fixed NdFeB content but different carbonyl iron concentration are considered. The magnetomechanical model is developed based on the finite-strain theory assuming the plane-stress approximation of the two-dimensional cantilever of infinite width. The magnetic energy comprises two magnetic terms, one of which is qualitatively linear and the other one is quadratic in the applied field strength. The numerically calculated field-programmed equilibrium bending shapes of the cantilevers are compared with the experimentally observed shapes. The model provides good agreement with the experiment up to moderate concentrations of the MS filler, when the coefficients of customary interpolation formulas for the concentration dependencies of elastic modulus and magnetic susceptibility are properly adjusted.

* Authors to whom any correspondence should be addressed.

Original Content from this work may be used under the terms of the Creative Commons Attribution 4.0 licence. Any further distribution of this work must maintain attribution to the author(s) and the title of the work, journal citation and DOI.

Keywords: magnetoactive elastomer, mixed magnetic filler, cantilever, bending deformation, shape-programmability, remanent magnetisation

(Some figures may appear in colour only in the online journal)

1. Introduction

Magnetoactive elastomers (MAEs) are a special type of smart materials consisting of soft elastic matrices filled with micron-sized ferromagnetic particles. They are becoming widely accepted as materials for vibration protection [1–5], damping, acoustic shielding [6] as well as for the manufacture of grippers and actuators in macro- and microrobotics [7–11]. An MAE cantilever, which is a rod rigidly fixed at one end, besides being an important piece of many of the above-mentioned devices, is the key element in designing the vibration and acceleration sensors based on MAEs. In case of an MAE cantilever, the advantage is that its properties can be strongly changed in a contactless manner by applying a magnetic field, and its deformation can be directly converted into an electromagnetic induction signal and transmitted to a measuring or control circuit.

The bending of the cantilever is a convenient parameter for monitoring in statics, while in dynamics the most convenient parameters are the amplitude-frequency characteristics caused by the bending oscillations of the cantilever. Two operating modes of the MAE-based cantilever sensor can be purposefully selected: (a) one can analyse the characteristics of external impulse disturbances by measuring the free oscillations of the cantilever, or (b) it is possible to realise a stationary oscillation mode of the cantilever and to monitor the evolution of the external conditions acting on the system by observing its parameters.

The prospect of application of MAE cantilevers in sensors spawns an interest in the theory of these structural elements, which requires obtaining an object-oriented set of equations that combines the mechanics of an elastic beam with Maxwell's equations for a continuous medium. Including magnetic terms, significantly affects the balance of internal forces in the MAE composite and, as a result, greatly changes the response characteristics of the cantilever to external mechanical and/or magnetic stimuli. Magnetomechanical contributions that describe mesoscopic (between particles inside the MAE) and macroscopic (cantilever as a whole with an applied field) interactions introduce a significant non-linearity into the problem. Therefore, numerical simulations have become one of the leading approaches to estimate the main parameters of such systems required for their destination application.

For any MAE sensor, and a cantilever in particular, the choice of the material is a crucial factor since modern MAEs are very diverse in composition and internal structure, and therefore differ significantly from each other in their physical properties. The two most important characteristics that predetermine their field-dependent behaviour are the type of dispersed ferromagnetic filler (either magnetically soft (MS), magnetically hard (MH), or a mixture of those) and the structural organisation of particles at the mesoscopic level. Indeed, the particle arrangement is formed at the polymerisation stage of the MAE synthesis and may be varied from isotropic spatial distribution (no external field) to a pronounced anisotropic structure (preliminary texturing) when polymerisation is performed in the presence of an external magnetic field. Moreover, unlike an MAE with MS filler (we term it MAE-MS), an MAE with MH filler (we term it MAE-MH), even if spatial distribution of the particles is homogeneous, may be (and usually is) made magnetically anisotropic after polymerisation by magnetising it by imposing a strong field, i.e. forcibly orienting the particle magnetic moments by internal switching. Clearly, for a cantilever made of a magnetised MAE-MH, both static and dynamic responses to applied forces or magnetic fields depend on how its internal anisotropy is directed with regard to the cantilever body.

The diversity of MAEs in material composition and structure leads to the fact that specialised models are required to describe different types of cantilevers. In general, by nowadays in the literature there are numerous works devoted to theoretical and experimental problems of MAE cantilevers, On the other hand, if one is interested in considering a specific type of cantilever—in our case these are cantilevers made of MAEs of mixed MH+MS content—it turns out that the reliable pertinent information on that is scarce and, often, insufficient.

By now, the main amount of knowledge has been accumulated on the cantilevers made of MAEs-MS, they were the first to become a focus of interest. One may find detailed experimental data [12–21] together with numerous publications on the theory and numerical simulation [17, 18, 22, 23]. The given references are just examples, the full list is far too long. As in the vast majority of those papers only quasi-static problems are addresses and solved, we would like to separately note the works on the behaviour of soft MAE cantilevers in alternating magnetic fields [24, 25].

The area of scientific interest is now shifting towards MAEs-MH where the MH particles are an order of magnitude larger in size than the MS particles. These composites together promise to yield more sensitive sensors, and also possess additional, tuneable custom parameters [26–29]. The theoretical and experimental studies of these objects is rapidly developing [27, 30–38].

Meanwhile, yet the next generation of MAE sensors seems to be cantilevers made of composites of mixed content, where the magnetic filler is two-component: comprising MS (e.g. carbonyl iron) and MH (e.g. NdFeB) micron-sized particles. In these materials (we term them MAEs-MC), the MS phase is responsible for a high magnetic susceptibility, and the MH phase is responsible for the presence of

remanent magnetisation which exists even in the absence of an external field [39–43]. In this case, another tuneable parameter appears—the relative ratio of fillers. Moreover, an MAE-MC cantilever may be made re-programmable by tuning its elastic modulus and remanent magnetisation with the aid of external field [28].

The specifics of MAEs-MC is that therein both filler components always affect each other since they are inherently coupled by magnetic interaction, which works in a rather complicated way [44]. In such a system two opposite tendencies compete. On the one hand, the MS phase shields, and thereby weakens, the magnetic field of each MH particle. On the other hand, as the MS particles fill in the space between the usually much larger MH particles, they turn out to serve as mesoscopic magnetic circuits with a high saturation magnetisation that entail an increase of the macroscopic magnetisation of the sample. The predominance of one tendency over the other is ensured, of course, by the relative content of the fillers.

This paper studies the bending deformation of horizontal MAE-MC cantilevers in a vertical uniform magnetic field. The objects of study are the permanently magnetised cantilevers of the same geometry but with different proportion between the MH and MS phases. In section 2, the finite-strain theory is introduced to derive the energy density function of the MAE-MC under large deformations. The magnetic filler contributions to the magnetic energy are assumed to be additive, where one term (MH) is linear in the applied field strength due to the remanent magnetisation and the other term (MS) is quadratic to the field owning to a high magnetic susceptibility. Section 3 presents the plane-stress model approximation of the two-dimensional (2D) MAE-MC cantilever of infinite width and the numerical solution of the variational problem using the finite element method (FEM). The experimental section 4 describes the synthesis of the MAE-MC cantilevers and the setup for measuring their field-programmable equilibrium bending shapes. The comparative analysis of the numerical simulation results with the experimental data is provided in section 5. The final section is devoted to a discussion of the results.

2. Magnetomechanics of an MAE cantilever

The equilibrium shape of an MAE cantilever in a magnetic field is determined by the balance of magnetostatic, elastic and gravitational forces distributed over the material volume. The scientific problem of a magnetised horizontal cantilever in the presence of a uniform magnetic field $\boldsymbol{H}_0$ generally contains three orientation parameters: two angles that the main cantilever axis $\boldsymbol{n}$ makes with the gravity direction $\boldsymbol{g}$ and with the applied field, as well as the angle between the directions of the remanent magnetisation $\boldsymbol{M}_\mathrm{r}$ and the field $\boldsymbol{H}_0$. As a rule, the cantilever is magnetised along the length axis, so that it is formed in a state where vectors $\boldsymbol{M}_\mathrm{r}$ and $\boldsymbol{n}$ are parallel. Given a high magnetic rigidity of the particles and their strong bonding to the polymer matrix, we assume that this juxtaposition of the directions is not lost when the cantilever is bent. Below, we consider the problem of a horizontal MAE cantilever in the field $\boldsymbol{H}_0$ parallel to $\pm\boldsymbol{g}$ that has only one essential orientation parameter, which is the angle between $\boldsymbol{n}$ and $\boldsymbol{H}_0$.

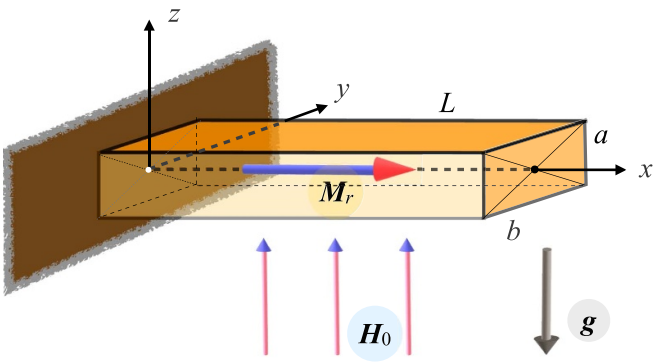

Figure 1. Schematic of the MAE-MC cantilever with the remanent magnetisation along the length axis; the directions of gravity and a would-be imposed uniform magnetic field are indicated.

2.1. Beam approximation for a composite non-magnetic cantilever

In classical mechanics, the bending theory of a non-magnetic cantilever is well developed, see [45–47], for example. As a zero-approximation, let us recall the well-known result of the linear theory of elasticity describing the bend of a horizontal cantilever with length L, width b and thickness a in the gravity field, see figure 1. If the bend is relatively small compared to the cantilever length, the vertical displacement of the free end is expressed by the formula [48]:

$$u_z^{\mathrm{end}} = -\rho g L^4/2Ga^2, \tag{1}$$

where g is the gravitational acceleration, G is the shear modulus of the material, and ρ is its mass density assuming that the cantilever material is fully homogeneous. Here, the origin of the Cartesian coordinate system $Oxyz$ is positioned at the fixed support, whereas Oz is the direction of $-\boldsymbol{g}$.

In our case, the MAE cantilever material is a composite, that is, a polymer matrix with density of ρ_m, in which spherical magnetic filler particles of density ρ_p are distributed with volume concentration ϕ. Then the MAE density is a linear combination of the partial components: $\rho = (1-\phi)\rho_m + \phi\rho_p$. For small and moderate values of ϕ ($\sim$30%), the shear modulus may be approximated by the well-known relation from the theory of isotropic composites derived for randomly distributed spherical particles [49]:

$$G = G_0\left(1 + \frac{16-15\nu}{2(4-5\nu)}\phi + q\frac{15(1-\nu)}{2(4-5\nu)}\phi^2\right), \tag{2}$$

that is exact with the ϕ^2 accuracy; here G_0 is the shear modulus of the unfilled matrix, ν is the Poisson's ratio, and q is the fitting coefficient depending on the type of the particle distribution.

Substitution of equation (2) into formula (1) shows that the gravitational sagging of the cantilever decreases as the filler concentration increases: $u_z^{\mathrm{end}} \propto \phi^{-1}$. This means that the

material stiffening prevails over the increase of its specific gravity. Obviously, this conclusion for the MAE cantilever is fully correct only in the absence of an external magnetic field. When the field is turned on, the ferromagnetic component contribution significantly interferes with the balance of competing elastic and gravitational forces.

2.2. Finite-strain description

In practice, the cantilever bending is not necessarily small and therefore needs to be described by the theory of finite elastic deformations. Consider two body configurations: initial undeformed and current deformed (actual) ones. The radius vector of an arbitrary point is denoted as $\boldsymbol{r}$ in the initial configuration and as $\boldsymbol{R} = \boldsymbol{r} + \boldsymbol{u}$ in the current configuration, where $\boldsymbol{u}$ is the displacement vector. The basis vectors of the local coordinate system in the initial configuration are $\boldsymbol{\epsilon}_i = \partial \boldsymbol{r} / \partial q^i$. Their counterparts in the current configuration are $\hat{\boldsymbol{\epsilon}}_i = \partial \boldsymbol{R} / \partial q^i$, where q^i are the generalised coordinates.

The Hamilton operators $\nabla = \boldsymbol{\epsilon}^i \partial / \partial q^i$ of the initial configuration and $\hat{\nabla} = \hat{\boldsymbol{\epsilon}}^i \partial / \partial q^i$ of the current configuration are defined in terms of reciprocal basis vectors.

The fundamental kinematic quantity—the deformation gradient tensor—is expressed as

$$\mathbf{F} = (\nabla \boldsymbol{R})^{\mathrm{T}} = \hat{\boldsymbol{\epsilon}}_i \boldsymbol{\epsilon}^i = \mathbf{I} + (\nabla \boldsymbol{u})^{\mathrm{T}}, \tag{3}$$

where $\mathbf{I}$ is the metric unit tensor, and the tensor transposition is indicated by superscript T. The inverse of the deformation gradient tensor has the form

$$\mathbf{F}^{-1} = (\hat{\nabla} \boldsymbol{r})^{\mathrm{T}} = \boldsymbol{\epsilon}_i \hat{\boldsymbol{\epsilon}}^i = \mathbf{I} - (\hat{\nabla} \boldsymbol{u})^{\mathrm{T}}. \tag{4}$$

To describe rotary displacements, it is convenient to use the polar decomposition of the deformation gradient tensor

$$\mathbf{F} = \mathbf{O} \cdot \mathbf{U}, \tag{5}$$

where $\mathbf{O}$ is the orthogonal rotation tensor and $\mathbf{U}$ is the symmetrical tensor of pure strain, e.g. $\mathbf{O}^{\mathrm{T}} = \mathbf{O}^{-1}$ and $\mathbf{U}^{\mathrm{T}} = \mathbf{U}$.

The Hamilton operators in the current and initial configurations are related by

$$\hat{\nabla} = \mathbf{F}^{-\mathrm{T}} \cdot \nabla, \qquad \text{where} \qquad \mathbf{F}^{-\mathrm{T}} \equiv (\mathbf{F}^{\mathrm{T}})^{-1}. \tag{6}$$

The general form of the elastic energy density for a medium, which is isotropic in the initial state, is

$$W_{\mathrm{el}} = W_{\mathrm{el}}\big(\mathcal{I}_1, \mathcal{I}_2, \mathcal{I}_3\big), \tag{7}$$

where $\mathcal{I}_1 = \mathrm{tr}(\mathbf{C})$, $\mathcal{I}_2 = \frac{1}{2}\left[(\mathrm{tr}(\mathbf{C}))^2 - \mathrm{tr}(\mathbf{C}^2)\right]$ and $\mathcal{I}_3 = \det(\mathbf{C})$ are the principal invariants of the right Cauchy–Green deformation tensor $\mathbf{C} = \mathbf{F}^{\mathrm{T}} \cdot \mathbf{F}$.

We consider W_{el} in the form of the Peng–Landel elastic potential [50], in which the effects of the distortional and volume changes are clearly separated. It is known to be well appropriate for slightly compressible elastomers under large deformations. In the absence of magnetic field, this potential has the form

$$W_{\mathrm{el}} = \frac{1}{2} G \left(J^{-2/3} \mathrm{tr}(\mathbf{C}) - 3 \right) + \frac{1}{2} K (J-1)^2, \tag{8}$$

where K is the bulk modulus, which for a silicone rubber is much higher than the shear modulus G. The MAE of the considered type—a silicone rubber filled with metal particles—under the moderate loads behaves as a virtually incompressible medium: see [51], for example where the experimentally found Poisson ratio for a similar composite is greater than 0.49 at the magnetic phase volume fractions up to 50 vol.%. Given that, we simplify the Jacobian of deformation gradient tensor $J = \det(\mathbf{F})$ to $J \approx 1$.

The total energy of a magnetoelastic medium is defined according to [52] by

$$U = \int_{\Omega_{\mathrm{MAE}}} \rho f(\mathbf{F}, \boldsymbol{H}) \mathrm{d}V - \frac{1}{2} \mu_0 \int_{\Omega} H^2 \mathrm{d}V. \tag{9}$$

Here, μ_0 is the vacuum permeability, Ω is the entire computational volume and Ω_{MAE} is the MAE volume, both quantities defined with respect to the current configuration. Note that the energy density $f(\mathbf{F}, \boldsymbol{H})$ comprises the elastic contribution (equation (8)) as well. In the absence of conduction currents, the relation between internal magnetic field $\boldsymbol{H}$ in the material and externally applied field $\boldsymbol{H}_0$ is established by introducing scalar magnetostatic potential ψ. Expressing this relation in terms of the deformation gradient tensor in the current configuration, it takes the form of $\boldsymbol{H} = \boldsymbol{H}_0 - \hat{\nabla} \psi$.

The magnetisation and the Cauchy stress tensor of the considered magnetoelastic medium are determined by the derivatives of the energy density:

$$\boldsymbol{M} = -\frac{\rho}{\mu_0} \frac{\partial f}{\partial \boldsymbol{H}}, \qquad \mathbf{T} = \rho \mathbf{F} \cdot \frac{\partial f}{\partial \mathbf{F}}. \tag{10}$$

Note that all the quantities in expressions (9) and (10) refer to the current deformed configuration. Since this configuration is not known before the boundary value problem is solved, we transform the integrands in equation (9) to the initial configuration. The magnetic fields in the initial configuration are related according to $\boldsymbol{H} = \boldsymbol{H}_0 - \mathbf{F}^{-\mathrm{T}} \cdot \nabla \psi$. The density and the volume element are transformed from the initial configuration to the current configuration as $\rho = J^{-1} \rho_0$ and $\mathrm{d}V = J \mathrm{d}V_0$. In these notations, expression (9) takes the form

$$U = \int_{\Omega^{(0)}_{\mathrm{MAE}}} \rho_0 f(\mathbf{F}, \boldsymbol{H}) \mathrm{d}V_0 - \frac{1}{2} \mu_0 \int_{\Omega^{(0)}} J H^2 \mathrm{d}V_0, \tag{11}$$

where superscript '(0)' denotes the entire computational and the MAE volumes in the initial configuration, respectively. The displacement vector $\boldsymbol{u}$, and through it the deformation gradient tensor $\mathbf{F}$ are defined in the volume $\Omega^{(0)}_{\mathrm{MAE}}$, whereas field variables $\mathbf{H}$ and ψ are defined in $\Omega^{(0)}$.

Splitting the energy density f into elastic, defined by equation (8), and magnetic parts

$$f = W_{\mathrm{el}} / \rho_0 + W_{\mathrm{mag}} / \rho, \tag{12}$$

we bring the total energy (equation (11)) to the form

$$U = \int_{\Omega^{(0)}_{\mathrm{MAE}}} (W_{\mathrm{el}} + JW_{\mathrm{mag}})\mathrm{d}V_0 - \frac{1}{2}\mu_0 \int_{\Omega^{(0)}} JH^2 \mathrm{d}V_0. \quad (13)$$

For a magnetised medium, the magnetic part of the energy density is given by the general expression

$$W_{\mathrm{mag}} = -\mu_0 \int_0^H \boldsymbol{M}(\boldsymbol{H}')\mathrm{d}\boldsymbol{H}', \quad (14)$$

which is applied under the assumption that the MH and MS filler contributions to the magnetisation of the magnetised MAE-MC are additive, and the MS filler follows a linear magnetisation law:

$$\boldsymbol{M}(\boldsymbol{H}) = \boldsymbol{M}_{\mathrm{r}} + \chi_0 \boldsymbol{H}. \quad (15)$$

Thus, the MH filler imparts to the MAE-MC composite a constant remanence $\boldsymbol{M}_{\mathrm{r}}$, whereas the MS filler is characterised by a constant magnetic susceptibility χ_0. Substituting equation (15) into equation (14), we find

$$W_{\mathrm{mag}} = -\mu_0 \left(\frac{1}{2}\chi_0 H^2 + \boldsymbol{M}_{\mathrm{r}} \cdot \boldsymbol{H} \right). \quad (16)$$

An MAE-MC cantilever is considered ready for tests and work after it had passed application of a strong magnetic field directed along its length axis. As a result, it acquires the remanent magnetisation $\boldsymbol{M}_{\mathrm{r}}$ that is uniform over the cantilever volume. Given tight embedding of the MH particles, this means that when the cantilever is bent, vectors $\boldsymbol{M}^{(0)}_{\mathrm{r}}$ and $\boldsymbol{M}_{\mathrm{r}}$ in the initial and current configurations are related to each other by a pure rotation transformation:

$$\boldsymbol{M}_{\mathrm{r}} = J^{-1}\mathbf{O} \cdot \boldsymbol{M}^{(0)}_{\mathrm{r}}. \quad (17)$$

To provide a formal continuation of the deformation gradient tensor $\mathbf{F}$ everywhere in the computational volume Ω, the volume $\Omega \backslash \Omega_{\mathrm{MAE}}$ surrounding the cantilever is assigned the elastic potential of the form (8) but this volume has no magnetic properties. On the one hand, this is a formal assumption necessary for the stability of the computational algorithm. On the other hand, physical considerations require that the result obtained should not depend on the elastic properties of the surrounding medium because in the experiment the cantilever is surrounded by air. The necessary compromise is achieved by assigning to the region $\Omega \backslash \Omega_{\mathrm{MAE}}$ a shear modulus G_{s}, which is several orders of magnitude lower than G. In our case the factor $A = G_{\mathrm{s}}/G = 10^{-5}$ is used.

Finally, the expression for numerical evaluation of the total energy takes the form

$$U = \int_{\Omega^{(0)} \backslash \Omega^{(0)}_{\mathrm{MAE}}} \left(AW_{\mathrm{el}} - \frac{1}{2}\mu_0 JH^2 \right) \mathrm{d}V_0 + \int_{\Omega^{(0)}_{\mathrm{MAE}}} \left(W_{\mathrm{el}} + JW_{\mathrm{mag}} - \frac{1}{2}\mu_0 JH^2 \right) \mathrm{d}V_0. \quad (18)$$

3. Bending of a 2D cantilever

According to the classical beam model (1), the cantilever bending does not depend on its width b. Although this result is true only for small deformations, it is reasonable to assume that for moderate bends, the dependence of u_z^{end} on the width b is weak as well. Based on this assumption, we consider acceptable to consider a 2D approximation, in which the MAE-MC cantilever of width b is replaced by a thin plate of infinite width made of the same material.

3.1. Plane-stress approximation

For the plate problem in question, the generalised coordinates q^i (see section 2.2) may be chosen to coincide with the Cartesian coordinates $Oxyz$, so that the bending deformation takes place in the xOz plane, see figure 1. The 2D cantilever deforms in a plane-stress state, so that the stress tensor components perpendicular to the xOz plane, i.e. along Oy direction, are zero all over the material volume. In this situation, large deformations are described by the displacement vector $\boldsymbol{u}$, which has only two components $u_x(x,z)$ and $u_z(x,z)$. Therefore, the components of the deformation gradient tensor assume the form

$$F_{ij} \equiv \delta_{ij} + \frac{\partial u_i}{\partial q^j} = \begin{pmatrix} 1 + \frac{\partial u_x}{\partial x} & 0 & \frac{\partial u_x}{\partial z} \\ 0 & 1 + e_{yy} & 0 \\ \frac{\partial u_z}{\partial x} & 0 & 1 + \frac{\partial u_z}{\partial z} \end{pmatrix}, \quad (19)$$

where δ_{ij} is the Kronecker delta.

The unknown variable e_{yy} characterising the strain in the Oy direction, generates additional equation

$$\frac{\partial W_{\mathrm{el}}}{\partial e_{yy}} = 0,$$

which corresponds to the stress component being equal to $T_{yy} = 0$.

3.2. Numerical solution

For numerical implementation, the energy functional (equation (18)) is rewritten in the dimensionless form using the shear modulus G as the unit of measure:

$$\overline{U} = \frac{U}{G} = \int_{\Omega^{(0)} \backslash \Omega^{(0)}_{\mathrm{MAE}}} \left(A\overline{W}_{\mathrm{el}} - \frac{1}{2}J\overline{H}^2 \right) \mathrm{d}V_0 + \int_{\Omega^{(0)}_{\mathrm{MAE}}} \left(\overline{W}_{\mathrm{el}} + J\overline{W}_{\mathrm{mag}} - \frac{1}{2}J\overline{H}^2 \right) \mathrm{d}V_0. \quad (20)$$

Here, for dimensionless magnetic variables, we introduce notations $\overline{\boldsymbol{H}} = \boldsymbol{H}\sqrt{\mu_0/G}$ and $\overline{\boldsymbol{M}} = \boldsymbol{M}\sqrt{\mu_0/G}$. The other dimensionless quantities and variables are $\overline{K} = K/G$, $\overline{W}_{\mathrm{el}} = \frac{1}{2}\left(J^{-2/3}\mathrm{tr}(\mathbf{C}) - 3\right) + \frac{1}{2}\overline{K}(J-1)^2$ and $\overline{W}_{\mathrm{mag}} = -\frac{1}{2}\chi_0\overline{H}^2 - \overline{\boldsymbol{M}}_{\mathrm{r}} \cdot \overline{\boldsymbol{H}}$. All calculations are performed for $\overline{K} = 150$. The length scale is based on the doubled cantilever thickness $2a$ as a unit, so that the dimensionless local displacement of the cantilever is $\overline{\boldsymbol{u}} = \boldsymbol{u}/(2a)$.

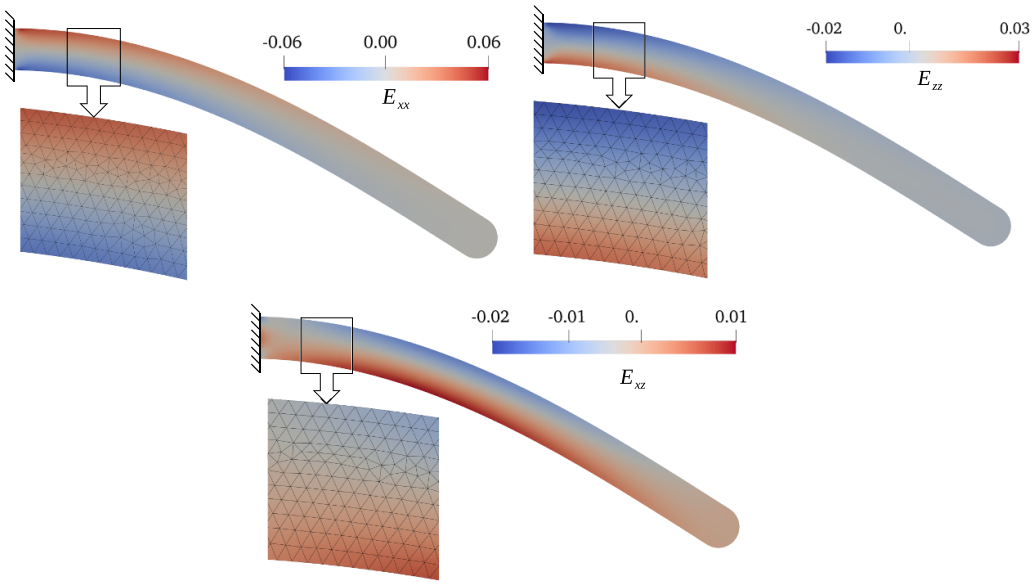

Figure 2. Distribution of the strain tensor components E_{xx}, E_{zz} and E_{xz} inside the model MAE cantilever with material parameters of the experimental MAE Sample No. 4 in an external field of $H_0 = -40\,\mathrm{kA\,m^{-1}}$.

Using the above-adopted notations, to describe the equilibrium problem, one has to solve the following variational equation together with the appropriate boundary conditions:

$$\delta\overline{U} = 0, \qquad \overline{\boldsymbol{u}}\big|_{x=0} = 0, \qquad \overline{\psi}\big|_{\Gamma_{\mathrm{ext}}} = 0, \tag{21}$$

where Γ_{ext} is the external boundary of the computational volume $\Omega^{(0)}$ and $\overline{\psi} = \psi\sqrt{\mu_0}/(2a\sqrt{G})$ is the dimensionless scalar magnetic potential. The solution is sought numerically by the FEM implemented by means of an open-source computer platform for solving partial differential equations FEniCS [53]. The mesh that covers the computational region consists of triangle elements and is generated automatically, an example is given in figure 2. The magnetostatic potential is approximated quadratically, whereas for the displacement vector a linear approximation is used. This FEM scheme is used to minimise the energy equation (20), i.e. to solve the quasistatic magnetoelastic problem, where the elastic and magnetic energy densities are rendered by equations (8) and (16), respectively. The numerical values of the material parameters are presented in sections 5.2 and 5.3.

The boundary conditions for the FEM model are given by equation (21). The mesh that covers the computational region consists of triangle elements and is generated automatically (see figure 2). The magnetostatic potential is approximated quadratically, whereas for the displacement vector a linear approximation is used. The FEM scheme implemented with the aid of FEniCS is used to minimise the energy equation (20), i.e. to solve the quasistatic magnetoelastic problem, where the elastic and magnetic energy densities are rendered by equations (8) and (16), respectively. The numerical values of the material parameters are presented in sections 5.2 and 5.3.

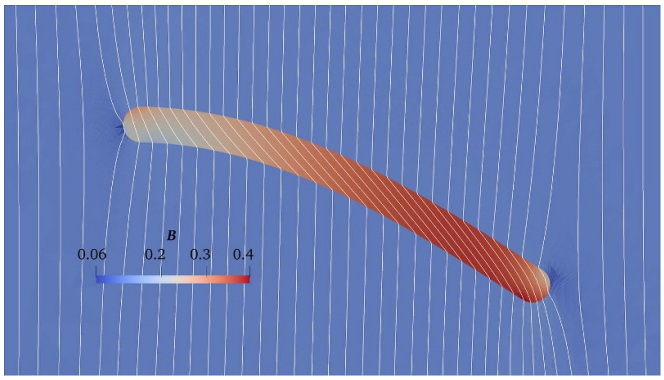

Figure 3. Distribution and field lines of the magnetic induction vector $\boldsymbol{B}$ inside and around the model MAE cantilever with material parameters of the experimental Sample No. 4 in an external field of $H_0 = -40\,\mathrm{kA\,m^{-1}}$. The colourmap indicates the magnitude of dimensionless magnetic induction $B/\sqrt{\mu_0 G}$.

The simulation results are exemplified in figures 2 and 3 for a model MAE cantilever whose material parameters correspond to the parameters of the experimental MAE Sample No. 4 described below: $G = 1.7\,\mathrm{MPa}$, $\chi_0 = 3.27$ and $M_{\mathrm{r}} = 35\,\mathrm{kA\,m^{-1}}$. The set of panels in figure 2 shows the distribution of three finite strain tensor components. This tensor is defined as $\mathbf{E} = \frac{1}{2}(\mathbf{C} - \mathbf{I})$ [54]. Unlike the customary strain tensor, it is applicable for the case of large deformations. In figure 3 the field distribution is presented in terms of the in-plane component of magnetic induction vector $\boldsymbol{B} = \mu_0(\boldsymbol{H} + \boldsymbol{M})$. The reason for the B-field representation is that it is more convenient for direct comparison with experimental field measurements around the cantilever.

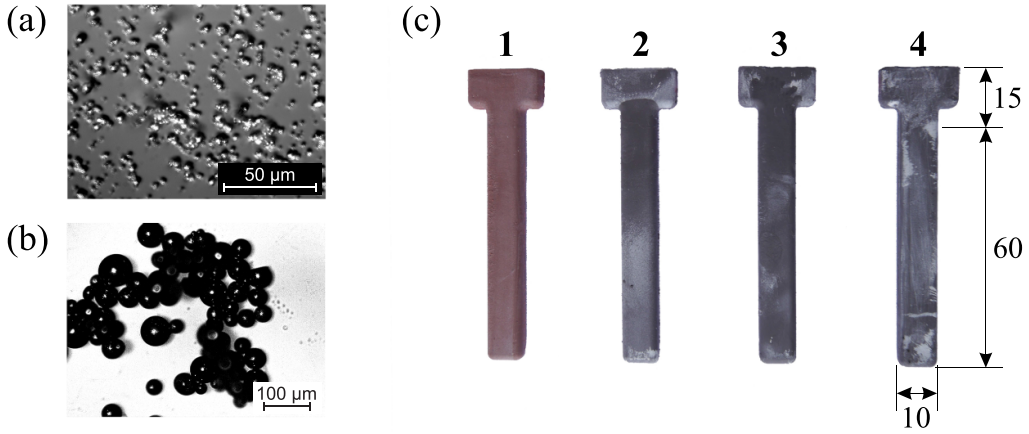

Figure 4. Microscopic images of (a) MS filler (BASF, grade CC) and (b) MH filler (Magnequench, MQP-S-11-9-20 001-070); (c) synthesised MAE cantilevers magnetised along the length, their dimensions are given in mm.

4. Experimental

4.1. MAE cantilever samples

The experimental study is carried out with a series of four MAE cantilevers of the same geometry but different material composition. The ingredients for the composite preparation are: a two-component silicone rubber Elastosil RT623 (Wacker Chemie AG, Germany) and two types of magnetic fillers. The MS filler consists of carbonyl iron powder (BASF, grade CC) with spherical particles of median diameter 3.8–5.3 μm [55]. For the MH filler, an NdFeB-alloy powder MQP-S-11-9-20001-070 (Magnequench) is used [56]. This powder contains micron-sized spherical particles with median diameter of 35–55 μm. Microscopic images of both powder types are shown in figures 4(a) and (b). The silicone density is $\rho_m = 1\,\mathrm{g\,cm^{-3}}$. The net density of the two-component magnetic filler defined as the weighted average between $\rho = 7.43\,\mathrm{g\,cm^{-3}}$ (Magnequench NdFeB, according to the manufacturer) and $\rho = 7.86\,\mathrm{g\,cm^{-3}}$ (carbonyl iron), so that the density of the solid phase ρ_m varies from $7.43\,\mathrm{g\,cm^{-3}}$ (Sample No. 1) to $7.56\,\mathrm{g\,cm^{-3}}$ (Sample No. 4); these values were used in the respective simulations. We note, however, that carbonyl iron micron particles are to some extent porous, and their degree of porosity is actually unknown. This means that ρ_m deviations between Samples Nos. 1 and 4 are actually even lower.

In the synthesis processes of each cantilever, the liquid silicone components are mechanically mixed with the required magnetic filler content. The magnetic composition is subjected to vacuuming to eliminate air cavities prior to polymerisation. This mixture is then poured into an aluminium mould and placed for curing at room temperature, being rotated on a loopster device at a rate of 10 rpm to prevent sedimentation of the magnetic filler.

Four synthesised MAE cantilever samples are presented in figure 4(c). The MH filler volume concentration in all cantilevers is maintained at a fixed value of 10%. The MS filler volume concentration is varied from 0% up to 30%. The magnetic composition of the cantilevers is summarised in table 1.

Table 1. Magnetic composition of the MAE cantilevers.

Sample No.	Magnetic filler type	ϕ_{MH}, vol%	ϕ_{MS}, vol%
1	MH	10	0
2	MH & MS	10	10
3	MH & MS	10	20
4	MH & MS	10	30

The cantilever No. 1 is made of an MAE with only MH filler, and therefore it is very different in colour due to the low magnetic filler concentration. Cantilevers Nos. 2–4 are of the MAEs-MC kind.

The cantilever geometric shape has a rectangular cross section of $a \times b = 5\,\mathrm{mm} \times 10\,\mathrm{mm}$ with edges rounded by a corner radius of 2 mm. The effective cantilever length (excluding fastening) is $L = 60\,\mathrm{mm}$. The T-shape end part is required for restraining the cantilever inside the fixed support. The same cantilever geometry has been used in our previous work [18], where we have studied the dynamic properties of vibrating soft magnetic cantilevers in order to utilise them as field-controlled sensor elements.

An important step after polymerisation is the magnetisation of all cantilevers in a pulse magnetic field of approximately 0.8 T to impart to them a remanent magnetisation. This is done in the electromagnet of Lake Shore 7407s magnetometer, where each cantilever is placed in such a way that its length axis is aligned parallel to the magnetising field.

4.2. Experimental setup

The MAE cantilever shape-programmable bending is investigated experimentally in a uniform magnetic field. This applied field H_0 is generated by a Helmholtz coil pair with a vertical axis. The coils are separated by a distance of 133 mm equal to their radius. A current in the coils generates an almost uniform magnetic field up to $\pm 40\,\mathrm{kA\,m^{-1}}$, which is directed either upward or downward depending on the current direction. The homogeneity of the field is proven by measurements in air with

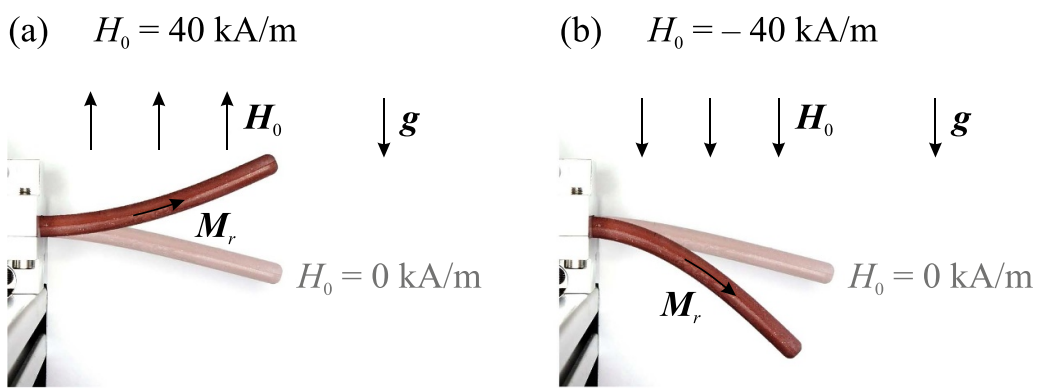

Figure 5. Programmed plane bending shape of the magnetised MAE cantilever No. 1 controlled by the application of a uniform magnetic field in comparison with the original shape caused by gravity: (a) $H_0 = 40\,\mathrm{kA\,m^{-1}}$, (b) $H_0 = -40\,\mathrm{kA\,m^{-1}}$.

a Hall sensor and simulated using the FEM in ANSYS software. Results of both tests render the magnetic field homogeneity not worse than 96.5% compared to the maximum field value in the relevant inner region between the coils.

Each cantilever is placed in the centre of the Helmholtz coil, so that its T-shaped part is rigidly clamped inside an aluminium fixed support. The initially undeformed straight Ox axis of the cantilever is horizontal and coincides with the middle axis between the coils. In the presence of gravity and applied magnetic field, which both act vertically, the cantilever bends in the xOz plane. The magnetic field-programmable deformation of the cantilever is measured using a laser triangulation sensor attached to a horizontal linear axis above the cantilever in the same vertical plane of bending. The laser sensor is driven by an external stepper motor with a constant speed of $10\,\mathrm{mm\,s^{-1}}$ in the Ox (horizontal) direction. When moving, the sensor measures vertical distance $z^{\mathrm{top}}_{\mathrm{exp}}(x)$ to the upper side of the cantilever all along its length. The output signal of the laser sensor together with the signal of the Hall sensor used for registration of the applied uniform field, is transmitted and analysed using a PC software. The temperature is kept at the room level. The influence of other experimental factors are not examined.

The bend measurements are carried out by applying five moderate field strengths H_0 between $-40\,\mathrm{kA\,m^{-1}}$ and $40\,\mathrm{kA\,m^{-1}}$ with increment $20\,\mathrm{kA\,m^{-1}}$. For all cantilevers, the occurring static bending is measured six times at each field magnitude. Before taking each next measurement within the series, the cantilever is turned over by 180° around its length axis and fastened anew in the fixed support. This variation of the two cantilever symmetrical orientations is done to exclude the effect of possible spatial non-uniformity of the magnetic filler inside the sample (e.g. due to the particle sedimentation during the MAE synthesis) on the measurement error. Based on six separate measurements, the average bending shape of the cantilever upper surface is evaluated for a given applied field strength. The standard deviation calculated for each set of tests is below 1.41 mm. Those averages as functions of ϕ_{MS} are plotted as dots in figures 8–11 below. The bending shapes of the MAE cantilever No. 1 with and without application of a uniform magnetic field of $H_0 = \pm 40\,\mathrm{kA\,m^{-1}}$ are compared in figure 5.

5. Testing the model against measurements

5.1. Functional approximation for the measurement data

To compare the experimental results with the theoretical model, the discrete set of measurements of the bent cantilever shapes is transformed into a continuous function $z(x)$ describing the bending of the cantilever middle line in the coordinate system shown in figure 1. Let us introduce the angle $\alpha(s)$ between the tangent to the cantilever middle line $z(x)$ and the Ox axis, where s is the natural length parameter varying from zero to L and counted from the fixed support: $s = 0$ for $x = 0$. The relations $\mathrm{d}x/\mathrm{d}s = \cos\alpha(s)$ and $\mathrm{d}z/\mathrm{d}s = \sin\alpha(s)$ take place at each point of the middle line. Their integration defines function $z(x)$ in parametric form. Assuming that the cross sections of the cantilever remain flat and normal to the middle line during deformation, the bending shape of the upper surface, which is measured in the experiment, is described by

$$x^{\mathrm{top}} = x - \frac{a}{2}\sin\alpha, \qquad z^{\mathrm{top}} = z + \frac{a}{2}\cos\alpha, \tag{22}$$

where a is the cantilever thickness.

For the tangent angle, the following polynomial approximation is taken

$$\alpha(s) = \alpha_0 + k_1 s/L + k_2(s/L)^2 + k_3(s/L)^3 + k_4(s/L)^4. \tag{23}$$

Here, a constant angle $\alpha(0) = \alpha_0$ independent of s is introduced in order to take into account the non-absolute rigidity of the cantilever fixed support in the experimental setup.

Coefficients α_0 and k_i in formula (23) are found by numerical minimisation of the discrepancy between function (23) and the measurement data: $||z^{\mathrm{top}} - z^{\mathrm{top}}_{\mathrm{exp}}|| \to \min$ for each MS filler concentration ϕ_{MS} and each applied field value H_0. As a result, for each of the four studied cantilevers, smooth interpolation functions of the measurement data are constructed approximating the experimental bending shapes with good accuracy for all field values, which is convenient for further comparison with the results of the numerical simulation.

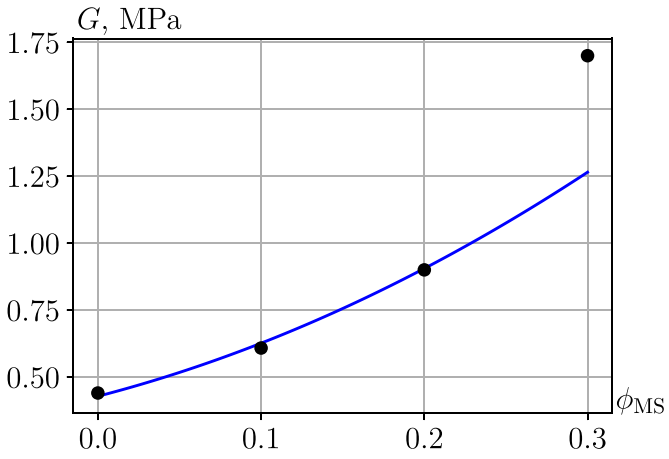

Figure 6. MS filler concentration dependency of the shear modulus. Result of experimental data fitting for $H_0 = 0$ is shown by markers, the interpolation result given by equation (2) for $G_0 = 310$ kPa and $q = 5.2$ is shown by solid line.

5.2. Estimation of the material parameters

The proposed continuum model (21) describes the MAE magnetomechanics using very few material parameters. The numerical values of these parameters are found by running test calculations in order to achieve the best agreement between the simulation results and the collected array of experimental data of cantilever deformation. In a preparatory step, the specified data are corrected by setting α_0 to zero to simulate an absolutely rigid cantilever fixation in the support. This allows us in all the further calculations to set the middle line $z(x)$ strictly perpendicular to the cross section plane yOz at $x = 0$.

Then, the values of the MAE elastic modulus and its dependence on ϕ_{MS} are determined. For that, the measurements of bent shapes of the cantilevers under their own weight are used. As these data are recorded under $H_0 = 0$, the interactions of the MAE with an external field are excluded. The experimental shapes are fitted in a series of numerical calculations, where the shear modulus G is the only variable parameter. The results obtained are represented by markers in figure 6. There is also a curve $G(\phi_{MS})$ calculated with the aid of formula (8) for $G_0 = 310$ kPa and $q = 5.2$. As seen, this analytical dependence describes the studied MAEs fairly well in the range $0 \leqslant \phi_{MS} \leqslant 0.2$. Note that formula (2) deals with the total concentration of the solid filler of the composite: $\phi = \phi_{MH} + \phi_{MS}$, so that $\phi_{MS} = 0.2$ in figure 6 corresponds to $\phi = 0.3$. The latter value is conventionally considered to be the applicability limit of the specified interpolation, so the disagreement at $\phi_{MS} = 0.3$ is quite expected.

To estimate the remanent magnetisation M_r brought in by the MH filler and the magnetic susceptibility χ_0 of the MS filler, we apply the following qualitative considerations. Let us recall that for all the studied cantilevers the content of the MH fillers is the same: $\phi_{MH} = 0.1$. For small cantilever deformations, the bending torque due to the constant magnetisation is of the order of $\sim\mu_0 M_r H_0$, i.e. is linear in M_r. On the other hand, the torque associated with the demagnetising field is proportional to $\mu_0\chi_0^2 H_0^2 u_z$, i.e. it becomes significant only for sufficiently large fields and bending. Assuming that the contribution of constant magnetisation dominates in the field $H = \pm 20\,\mathrm{kA\,m^{-1}}$, we assume $\chi_0 = 0$ and, by fitting the cantilever shapes, find the first approximation for function $M_r(\phi_{MS})$. As expected, calculating with this approximation the cantilever shapes in the field $H = \pm 40\,\mathrm{kA\,m^{-1}}$ yields deviations, which are definitely due to the contribution of the demagnetisation field. By iterating the value of χ_0, we achieve agreement between the results, and then refine M_r and χ_0 using the indicated iterative method based on the available experimental data of the cantilever shapes in the fields $\pm 20\,\mathrm{kA\,m^{-1}}$ and $\pm 40\,\mathrm{kA\,m^{-1}}$.

In figure 7 the markers show the values obtained according to the fitting scheme described above. The line in figure 7(a) is a linear dependence predicted in [44]. For these line parameters we obtain $M_r(\phi_{MS} = 0) = 21\,\mathrm{kA\,m^{-1}}$ and $\mathrm{d}M_r/\mathrm{d}\phi_{MS} = 49\,\mathrm{kA\,m^{-1}}$. The curve in figure 7(b) corresponds to the Lichtenecker-type effective medium approximation [57]:

$$\chi_0 = \chi_{MH} + \left(\mu_e^{\phi_{MS}/(1-\phi_{MH})} - 1\right). \tag{24}$$

Here, μ_e is the effective magnetic permeability of MS particles. Through experimental comparison $\mu_e = 70$ is obtained. Note that formula (24) rendering a complete model, includes the magnetic susceptibility of MH particles. However, according to the results of [44], the MH magnetic susceptibility is small, viz. $\chi_{MH} \simeq 0.03$, which therefore has little effect on the results. As seen in figure 7(b), formula (24) accurately describes the available measurements in the range $0 < \phi_{MS} < 0.2$. When the concentration increases to $\phi_{MS} = 0.3$ the accuracy decreases; notably, this is the same limit at which the interpolation dependence $G(\phi_{MS})$, see figure 6, loses its reliability.

5.3. Field-programmable cantilever deformation: model vs. experiment

The obtained material parameter values are dependent on the MS filler concentration. Taking these dependencies into account, we calculate field-programmable equilibrium shapes of MAE cantilevers with different magnetic content. These results are presented in figures 8–11. In each of the figures labelled (a), the solid lines show the numerically calculated cantilever contours in different applied uniform fields. The dotted lines represent the bent shapes of the cantilever upper surface obtained from smoothed experimental data, whereby setting the angle $\alpha_0 = 0$. In each of the figures labelled (b), the model predictions are compared with the real deviations of the cantilever end point from the magnetomechanical behaviour horizontal.

The model calculations quite satisfactorily describe the measurement results within the range $0 \leqslant \phi_{MS} \leqslant 0.2$, i.e. with the total amount of the solid filler $\phi \leqslant 0.3$. Noticeable

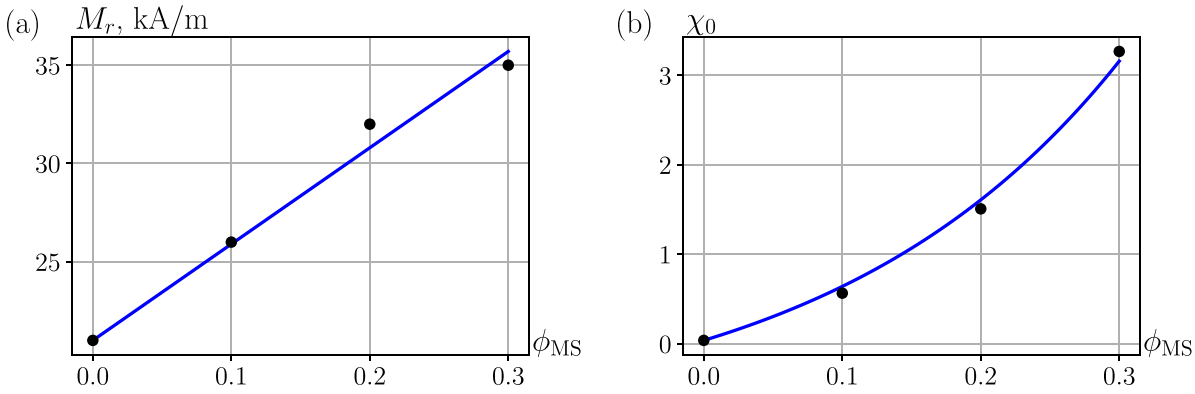

Figure 7. MS filler concentration dependencies of (a) remanent magnetisation and (b) magnetic susceptibility. Results of experimental data fitting for $H_0 = 0$ are shown by markers, the interpolation results are shown by solid lines.

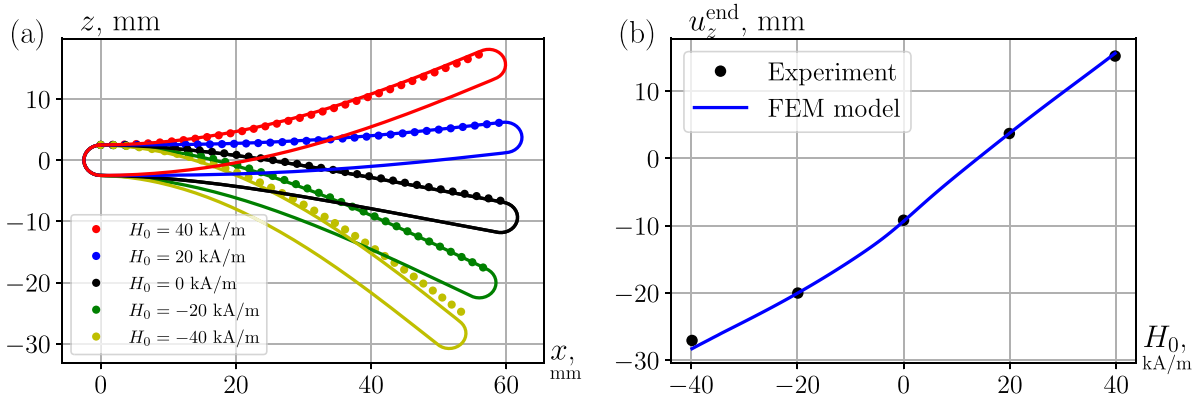

Figure 8. Comparison of model and experiment for the cantilever No. 1 filled only with MH particles ($\phi_{\mathrm{MH}} = 0.1$ and $\phi_{\mathrm{MS}} = 0$) in different applied fields: (a) numerically calculated cantilever contours are shown by solid lines, smoothed experimentally measured shapes of the cantilever upper surface are shown by dotted lines. (b) Field-dependent deflection of the cantilever end point.

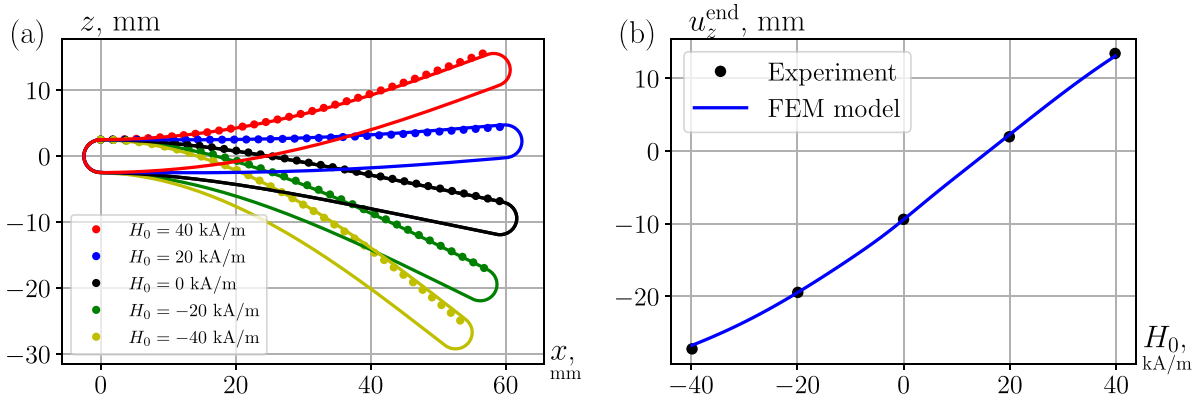

Figure 9. Comparison of model and experiment for the cantilever No. 2 of mixed content ($\phi_{\mathrm{MH}} = 0.1$ and $\phi_{\mathrm{MS}} = 0.1$) in different applied fields: (a) numerically calculated cantilever contours (solid lines), smoothed experimentally measured shapes of the cantilever upper surface (dotted lines). (b) Field-dependent deflection of the cantilever end point.

differences between the model predictions and the measurement results for $\phi \leqslant 0.4$ in a strong magnetic field are quite expected. Indeed, at such a high degree of composite filling, a simple model that characterises the MAE using a small number of material parameters can, at best, claim only qualitative agreement.

6. Results and discussion

Calculating the field-programmable deformation of the cantilevers made of MAEs-MC is a multifactorial problem for which the material parameters are not always known with satisfactory accuracy. These uncertainties are enhanced by the

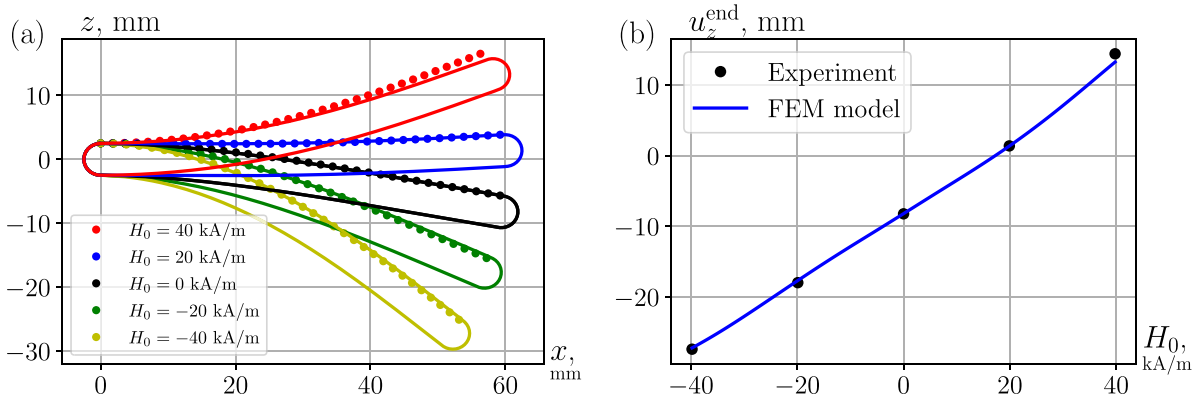

Figure 10. Comparison of model and experiment for the cantilever No. 3 of mixed content ($\phi_{\text{MH}} = 0.1$ and $\phi_{\text{MS}} = 0.2$) in different applied fields: (a) numerically calculated cantilever contours (solid lines), smoothed experimentally measured shapes of the cantilever upper surface (dotted lines). (b) Field-dependent deflection of the cantilever end point.

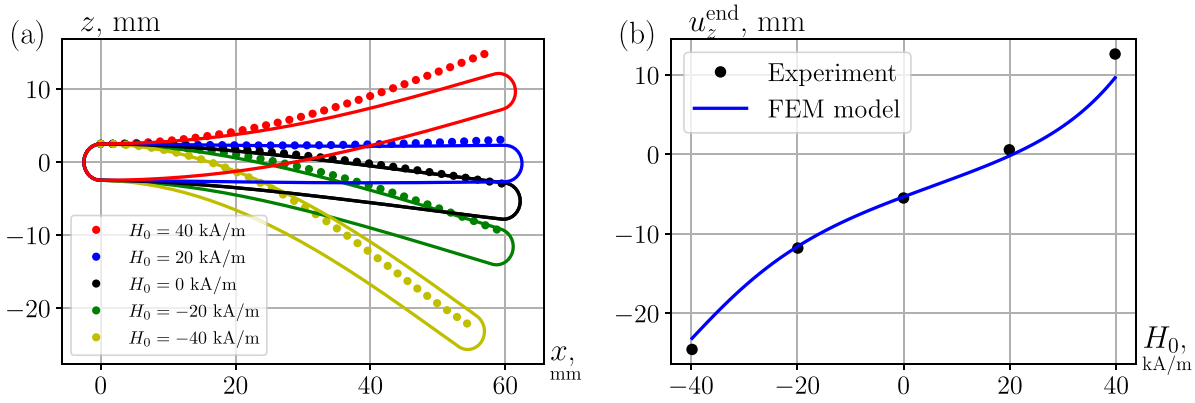

Figure 11. Comparison of model and experiment for the cantilever No. 4 of mixed content ($\phi_{\text{MH}} = 0.1$ and $\phi_{\text{MS}} = 0.3$) in different applied fields: (a) numerically calculated cantilever contours (solid lines), smoothed experimentally measured shapes of the cantilever upper surface (dotted lines). (b) Field-dependent deflection of the cantilever end point.

inevitable heterogeneity of material properties, occurring at the stage of composite synthesis. For this reason, there are no grounds to expect that the constructed macroscopic models would ensure very high accuracy, at least at the current stage of development of MAE material science.

Nevertheless, the developed model shows that, based on the fundamental relations of mechanics and physics, it is possible to substantiate comparably simple but sufficiently robust approximations which reflect correctly the main properties of MAEs-MC. This advances the understanding of the behaviour of these complex material systems. As figures 8–11 show, our model is able to correctly describe the magnetic field-induced deformation behaviour of cantilevers made of the elastomers which differ significantly in the degree of magnetic filling.

The model numerical calculations render the deformed equilibrium shapes of MAEs quite close to those observed in experiment and cover a range of relative concentrations of the solid phases. We note that the magnetic response of MAE-MC cantilevers up to now has not been studied by anyone, although the magnetomechanical behaviour of the samples filled with monophase—either MS or MH—fillers were explored extensively.

It was quite reasonable to infer that a more dense filling of the composite with MS particles that have a high magnetic susceptibility should markedly increase the response of the cantilever that in our case is the deviation of the cantilever end from the horizontal. However, the theoretical analysis, performed and experimentally verified, shows that the increasing modulus of elasticity of the material, that is, its ability to resist forced deformation, actually compensates the effect of the enhanced magnetisation. From the evidence obtained on the set of four MAE-MC cantilevers studied under the fields up to $\pm 40\,\text{kA}\,\text{m}^{-1}$, one concludes that their inflection is mainly caused by the presence of the MH filler whose volume fraction is the same in all the cantilevers. In other words, adding the MS filler, even in significant amounts, has almost no effect on the resulting bending deformation.

On the other hand, the degree of MS filling affects the differential susceptibility $\mathrm{d}u_z^{\text{end}}/\mathrm{d}H_0$ for cantilevers with different concentration values ϕ_{MS}. Whereas this susceptibility is practically constant for a cantilever with a low amount of the MS phase, for a highly filled cantilever it increases noticeably as the applied field grows, see figures 8(b) and 11(b).

It is important to emphasise that, a part of particular results on the equilibrium shapes of MAE-MC cantilevers,

the presented work implies, in our view, a much more general result. Namely, we have shown that the material parameters of an MAE-MC can be successfully described by known approximation formulas up to moderate concentrations of the MS filling. The obtained results also confirm the conclusion first established in [44] that there is a linear dependence of remanent magnetisation on the MS filler concentration.

Certainly, the agreement between experiment and theory is not perfect. The occurring deviations may be due to a number of fundamental as well as particular causes. First place, it is the geometric simplification: the magnetostatic calculations are performed on a 2D model for a plate of infinite width instead of a real 3D beam model. Another important reason for deviation is the inapplicability of both the Peng–Landel potential (equation (8)) and the effective medium theory (equation (24)) for a highly filled elastomer, as it clearly follows from figures 6 and 7. The angular correction α_0 introduced into the model in equation (23) most probably does not fully take into account the influence of orientation misalignments inside the fixed cantilever support. It is reasonable to assume that some imperfection of the experimental setup has a deeper effect on the magnetomechanical response of MAE cantilevers, since there is hardly a way to completely eliminate the angle deviations of the sample in the clamp. Another factor that is difficult to take into account in modelling is a certain heterogeneity of the spatial distributions of both fillers inside the MAE-MC. Such an imperfection in the synthesis process is quite expected and just as fundamentally irremovable. At the same time, the obtained discrepancies between the developed model and the experiment are relatively small. This proves that the reliability of the model may be justly considered as satisfactory, at least from the point of view of applying this framework to engineering applications.

In conclusion, we remark that the case of cantilevers considered in this work is just a particular example. This developed framework with few material parameters may be applied to any MAE-MC of application interest, e.g. membranes, pipes, helixes, etc. On the other hand, at least one shortcoming of the above-presented cantilever problem is yet to be addressed. Whatever reasonable are the predictions of a 2D model, this should be compared against the 3D solution to estimate the limits of applicability. This is the issue to be focused on in the near future. This would bring a final justification of the static (equilibrium) aspect of the problem. With respect to applications, this scope is relevant for understanding functionality of slow-working MAE actuators and sensors like those discussed and shown in [58] where the MAE-MC content is formed by orientationally ordered iron nanowires so that MH and MS properties are integrated in one and the same object. Another essential aspect in which the work on MAE-MC is planned to be advanced is their dynamics. The use of cantilevers as accelerometers or vibration sensors requires understanding of field-tuning of their vibration frequency spectra and the quality factors of those oscillations.

Data availability statement

The data that support the findings of this study are available upon reasonable request from the authors.

Acknowledgments

T B, D B and K Z gratefully acknowledge the financial support by the Deutsche Forschungsgemeinschaft (DFG) through Projects BE-6553/2-1 and BO 3343/3-1. A B, Yu R, O V S and O S S are grateful for the financial support from the Russian Foundation for Basic Research (RFBR) under Project # 19-52-12045.

ORCID iDs

T I Becker https://orcid.org/0000-0003-2473-1599
D Yu Borin https://orcid.org/0000-0003-3842-1487
Yu L Raikher https://orcid.org/0000-0002-6167-6528

References

[1] Ubaidillah, Sutrisno J, Purwanto A and Mazlan S A 2015 Recent progress on magnetorheological solids: materials, fabrication, testing and applications *Adv. Eng. Mater.* **17** 563–97
[2] Böse H, Gerlach T and Ehrlich J 2021 Magnetorheological elastomers—an underestimated class of soft actuator materials *J. Intell. Mater. Syst. Struct.* **32** 1550–64
[3] Lucarini S, Hossain M and Garcia-Gonzalez D 2022 Recent advances in hard-magnetic soft composites: synthesis, characterisation, computational modelling and applications *Compos. Struct.* **279** 114800
[4] Moreno-Mateos M A, Hossain M, Steinman P and Garcia-Gonzalez D 2022 Hybrid magnetorheological elastomers enable versatile soft actuators *Comput. Mater.* **8** 162
[5] Choi Y T and Wereley N M 2022 Adaptively tunable magnetorheological elastomer-based vibration absorber for a propeller aircraft seat *AIP Adv.* **12** 035332
[6] Yu K, Fang N X, Huang G and Wang Q 2018 Magnetoactive acoustic metamaterials *Adv. Mater.* **30** 1706348
[7] Zimmermann K, Naletova V A, Zeidis I, Turkov V A, Kolev E, Lukashevich M V and Stepanov G V 2007 A deformable magnetizable worm in a magnetic field—a prototype of a mobile crawling robot *J. Magn. Magn. Mater.* **311** 450–3
[8] Lum G Z, Ye Z, Dong X, Marvi H, Erin O, Hu W and Sitti M 2016 Shape-programmable magnetic soft matter *Proc. Natl Acad. Sci.* **113** E6007–15
[9] Hu W, Lum G Z, Mastrangeli M and Sitti M 2018 Small-scale soft-bodied robot with multimodal locomotion *Nature* **554** 81–85
[10] Kim Y, Parada G A, Lui S and Zhao X 2019 Ferromagnetic soft continuum robots *Sci. Robot.* **4** eaax7329
[11] Bastola A K and Hossain M 2021 The shape-morphing performance of magnetoactive soft materials performance *Mater. Des.* **211** 110172
[12] Zrínyi M, Szabó D and Kilian H-G 1998 Kinetics of the shape change of magnetic field sensitive polymer gels *Polym. Gels Netw.* **6** 441–54
[13] Nikitin L V, Mironova L S, Stepanov G V and Samus A N 2001 The influence of a magnetic field on the elastic and

viscous properties of magnetoelastics *Polym. Sci.* A **43** 443–50
[14] Farshad M and Benine A 2004 Magnetoactive elastomer composites *Polym. Test.* **23** 347–53
[15] Ramanujan R V and Lao L L 2006 The mechanical behavior of smart magnet-hydrogel composites *Smart Mater. Struct.* **15** 952–6
[16] Miedzińska D and Slawiński G 2010 Numerical simulation of the beam made of magnetorheological elastomer bending in the magnetic field *J. KONES Powertrain Transp.* **17** 261–5
[17] Gao W, Wang L, Wang X and Liu H 2016 Magnetic driving flowerlike soft platform: biomimetic fabrication and external regulation *ACS Appl. Mater. Interfaces* **8** 14182–9
[18] Becker T I, Raikher Y L, Stolbov O V, Böhm V and Zimmermann K 2017 Dynamic properties of magneto-sensitive elastomer cantilevers as adaptive sensor elements *Smart Mater. Struct.* **26** 095035
[19] Becker T I, Böhm V, Chavez Vega J, Odenbach S, Raikher Y L and Zimmermann K 2019 Magnetic-field-controlled mechanical behavior of magneto-sensitive elastomers in applications for actuator and sensor systems *Arch. Appl. Mech.* **89** 133–52
[20] Birster K, Schweitzer R, Schopphoven C and Tschöpe A 2021 Field-induced deformation of ferromagnetic soft nanocomposites *J. Appl. Phys.* **55** 075003
[21] Kalita V M, Dzhezherya Y I, Cherepov S V, Skirta Y B, Bodnaruk A V and Levchenko G G 2021 Critical bending and shape memory effect in magnetoactive elastomers *Smart Mater. Struct.* **30** 025020
[22] Liu Y, Chen S, Tan X and Cao C 2020 A finite element framework for magneto-actuated large deformation and instability of slender magneto-active elastomers *Int. J. Appl. Mech.* **12** 2050013
[23] Barreto D D, Saxena S and Kumar A 2022 Numerical simulation of the beam made of magnetorheological elastomer bending in the magnetic field *Structures* **234–235** 111147
[24] Zimmermann K, Zeidis I, Naletova V A, Kalmykov S A and Turkov V A 2016 Model of a thin rod with viscoelastic magnetizable material in the alternating magnetic field *Solid State Phenom.* **190** 629–32
[25] Aguib S, Nour A, Djedid T, Bossis G and Chikh N 2016 Forced transverse vibration of composite sandwich beam with magnetorheological elastomer core *J. Mech. Sci. Technol.* **30** 15–24
[26] Zhou G Y and Jiang Z Y 2004 Deformation in magnetorheological elastomer and elastomer–ferromagnet composite driven by a magnetic field *Smart Mater. Struct.* **13** 309–16
[27] von Lockette P, Lofland S E, Biggs J, Roche J, Mineroff J and Babcock M 2011 Investigating new symmetry classes in magnetorheological elastomers: cantilever bending behavior *Smart Mater. Struct.* **20** 105022
[28] Borin D Y, Stepanov G V and Odenbach S 2013 Tuning the tensile modulus of magnetorheological elastomers with magnetically hard powder *J. Phys.: Conf. Ser.* **412** 012040
[29] Stepanov G V, Borin D Y, Bakhtiiarov A V and Storozhenko P A 2017 Magnetic properties of hybrid elastomers with magnetically hard fillers: rotation of particles *Smart Mater. Struct.* **23** 035060
[30] Sheridan R, Roche J, Lofland S E and von Lockette P 2014 Numerical simulation and experimental validation of the large deformation bending and folding behavior of magneto-active elastomer composites *Smart Mater. Struct.* **23** 094004
[31] Anderson K, Bravoco R, Hargrave W, Roche J, von Lockette P and Lofland S E 2015 Dynamic shear response of hard versus soft magnetic magnetoactive elastomers *Smart Mater. Struct.* **20** 025022
[32] Kramarenko E Y, Chertovich A V, Stepanov G V, Semisalova A S, Makarova L A, Perov N S and Khokhlov A R 2015 Magnetic and viscoelastic response of elastomers with hard magnetic filler *Smart Mater. Struct.* **24** 035002
[33] Zhao R, Kim Y, Chester S A, Sharma P and Zhao X 2019 Mechanics of hard-magnetic soft materials *J. Mech. Phys. Solids* **124** 244–63
[34] Lloyd P, Hoshiar A K, da Veiga T, Attanasio A, Marahrens N, Chandler J H and Valdastri P 2020 A learnt approach for the design of magnetically actuated shape forming soft tentacle robots *IEEE Robot. Autom. Lett.* **5** 3937–44
[35] Yan D, Abbasi A and Reis P M 2021 A comprehensive framework for hard-magnetic beams: reduced-order theory, 3D simulations and experiments *Int. J. Solids Struct.* **234** 111319
[36] Durastanti R, Giacomelli L and Tomassetti G 2021 Shape programming of a magnetic elastica *Math. Models Methods Appl. Sci.* **31** 675–710
[37] Kadapa C and Hossain M 2021 A unified numerical approach for soft to hard magneto-viscoelastically coupled polymers *Mech. Mater.* **166** 104207
[38] Sano T G, Pezzulla M and Reis P M 2022 A Kirchhoff-like theory for hard magnetic rods under geometrically nonlinear deformation in three dimensions *J. Phys. Mech. Solids* **160** 104739
[39] Borin D Y and Stepanov G V 2013 Oscillation measurements on magnetoactive elastomers with complex composition *J. Optoelectron. Adv. Mater.* **15** 249–53
[40] Linke J M, Borin D Y and Odenbach S 2016 First-order reversal curve analysis of magnetoactive elastomers *RSC Adv.* **6** 100407–16
[41] Odenbach S 2019 Microstructure and rheology of magnetic hybrid materials *Arch. Appl. Mech.* **89** 269–79
[42] Borin D, Stepanov G and Dohmen E 2019 Hybrid magnetoactive elastomer with a soft matrix and mixed powder *Arch. Appl. Mech.* **89** 105–17
[43] Borin D Y, Odenbach S and Stepanov G V 2019 Stress induced by the striction of hybrid magnetoactive elastic composites *J. Magn. Magn. Mater.* **470** 85–88
[44] Becker T I, Stolbov O V, Yu D Zimmermann B, K and Raikher Y L 2020 Basic magnetic properties of magnetoactive elastomers of mixed content *Smart Mater. Struct.* **29** 075034
[45] Svetlitsky V A 2005 *Dynamics of Rods* (Berlin: Springer)
[46] Beléndez T, Neipp C and Beléndez A 2002 Large and small deflections of a cantilever beam *Eur. J. Phys.* **23** 371–9
[47] Chen L 2010 An integral approach for large deflection cantilever beams *Int. J. Non-Linear Mech.* **45** 301–5
[48] Landau L D and Lifshitz E M 1986 *Theory of Elasticity* (Oxford: Butterworth-Heinemann)
[49] Chen H-S and Acrivos A 1978 The effective elastic moduli of composite materials containing spherical inclusions at non-dilute concentrations *Int. J. Solids Struct.* **14** 349–64
[50] Peng S T J and Landel R F 1975 Stored energy function and compressibility of compressible rubberlike materials under large strain *J. Appl. Phys.* **46** 2599–604
[51] Xu Y, Li M, Li H, Zhang S, Wang H, Guo X, Li T and Wu C 2021 The study on the mechanical properties of magnetorheological elastomers under triaxial compression *J. Intell. Mater. Syst. Struct.* **32** 1256–66

[52] Bustamante R, Dorfmann A and Ogden R W 2008 On variational formulations in nonlinear magnetoelastostatics *Math. Mech. Solids* **13** 725–45
[53] FEniCS Project 2019 (Version 2019.1.0) (available at: www.fenicsproject.org)
[54] Lurie A I 1990 *Nonlinear Theory of Elasticity* (Amsterdam: North-Holland)
[55] BASF Carbonyl iron powder (CIP), grade CIP CC (Product overview) (available at: https://docplayer.net/23874265-Carbonyl-iron-powder.html)
[56] Magnequench 2009 *MQP-S-11-9-20001-070 Isotropic Powder (Material Description)* (available at: https://mqitechnology.com/wp-content/uploads/2017/09/mqp-s-11-9-20001-070.pdf)
[57] Zakri T, Laurent J-P and Vauclin M 1998 Theoretical evidence for 'Lichtenecker's mixture formulae' based on the effective medium theory *J. Phys. D: Appl. Phys.* **31** 1589–94
[58] Alfadhel A and Kosel J 2015 Magnetic nanocomposite cilia tactile sensor *Adv. Mater.* **27** 7888–92